

- iodoamphetamine as a cerebral blood flow tracer using emission tomography. *J Nucl Med* 1990;31:1364-1369.
7. Yonekura Y, Nishizawa S, Mukai T, et al. Functional mapping of flow and back-diffusion rate of N-isopropyl-iodoamphetamine in human brain. *J Nucl Med* 1993;34:839-844.
 8. Yokoi T, Iida H, Itoh H, Kanno I. A new graphic plot analysis for cerebral blood flow and partition coefficient with iodine-123-iodoamphetamine and dynamic SPECT validation studies using oxygen-15-water and PET. *J Nucl Med* 1993;34:498-505.
 9. Iida H, Itoh H, Bloomfield PM, et al. A method to quantitate cerebral blood flow using a rotating gamma camera and iodine-123 iodoamphetamine with one blood sampling. *Eur J Nucl Med* 1994;21:1072-1084.
 10. Odano I, Ohkubo M, Takahashi N, Higuchi T. A new method of regional cerebral blood flow measurement using one-point arterial sampling based on the microsphere model with N-isopropyl-p-[¹²³I]-iodoamphetamine SPECT. *Nucl Med Commun* 1994;15:560-564.
 11. Kanno I, Uemura K, Miura S, Miura Y. HEADTOME: a hybrid emission tomograph for single photon and positron emission imaging of the brain. *J Comput Assisted Tomogr* 1981;5:216-226.
 12. Kanno I, Lassen NA. Two methods for calculating regional cerebral blood flow from emission computed tomography of inert gas concentrations. *J Comput Assisted Tomogr* 1979;3:71-76.
 13. Hoehn MM, Yahr MD. Parkinsonism: onset, progression and mortality. *Neurology* 1967;17:427-442.

Regional Differences in Technetium-99m-ECD Clearance on Brain SPECT in Healthy Subjects

Masanori Ichise, Haim Golan, James R. Ballinger, Douglass Vines, Adam Blackman and Harvey Moldofsky
Department of Nuclear Medicine, Mount Sinai Hospital; Department of Nuclear Medicine, Princess Margaret Hospital; Center for Sleep and Chronobiology, Toronto Western Division, The Toronto Hospital; and University of Toronto, Toronto, Ontario, Canada

The aim of this study was to evaluate the in vivo stability of ECD brain SPECT. **Methods:** Twenty normal volunteers (35.4 ± 9.1 yr) each had six ECD scans at 30, 60, 120, 240, 360 and 480 min postinjection. Each scan was acquired for 24 min using a triple-head SPECT system. Average counts per pixel were measured from frontal, temporal, parietal, occipital, cerebellum, basal ganglia, thalamus and white matter regions. ECD clearance rates were calculated by fitting regional time activity data to a monoexponential equation. Regional gray-to-white matter (G/W) and gray-to-cerebellum (G/C) ratios were calculated for each scan. Analysis of variance was used to compare regional ECD clearance and ratio measurements. **Results:** The average ECD clearance was 4.3%/hr. There was a significant regional variation in the ECD clearance, being higher for occipital (6.34%/hr) but lower for both white matter (2.39%/hr) and thalamus (2.45%/hr). Both G/W and G/C ratios showed a significant regional variation with time. The overall G/W ratio was 2.13 at 30 min and became progressively lower after 2 hr, reaching 1.78 at 8 hr. All regional G/W ratios declined with time except for thalamus where it remained constant at 2.15. The overall G/C ratio was 0.984 at 30 min but it declined after 4 hr, reaching 0.955 at 8 hr. All regional G/C ratios declined with time except for thalamus where it increased progressively from 0.955 to 1.120 at 8 hr. **Conclusion:** ECD clears from normal brain slowly and shows a significant regional variation. As a result, G/W contrast begins to decrease after 2 hr and the gray-matter activity pattern becomes significantly different after 4 hr. Therefore, the optimal imaging time may be between 30-120 min. However, images obtained up to 4 hr still maintain the initial gray-matter activity pattern.

Key Words: technetium-99m-ethyl cysteinate dimer; brain SPECT; regional cerebral blood flow

J Nucl Med 1997; 38:1253-1260

Tchnetium-99m-ethyl cysteinate dimer (ECD) is a relatively new ^{99m}Tc-labeled lipophilic tracer that became available clinically for SPECT imaging of regional cerebral blood flow (rCBF) (1). The clinical usefulness of ECD brain SPECT has been recently evaluated in several neurological conditions including cerebrovascular disease (2-6), dementia (7) and

epilepsy (8-10). Compared with the previously introduced ^{99m}Tc-HMPAO, ECD has a faster blood clearance providing more favorable radiation dosimetry and a higher signal-to-noise ratio (1) and is chemically stable in vitro for several hours after reconstitution (11). In contrast, HMPAO must be used within 30 min after reconstitution because the labeled compound rapidly decomposes in vitro (12) although a more stable formulation has been recently introduced. The purpose of this study was to evaluate another important property of ECD relevant to SPECT imaging, namely, its in vivo stability in the brain.

On intravenous injection, ECD like HMPAO crosses the blood brain barrier and becomes rapidly trapped in the brain in proportion to rCBF. The retention of the tracer in the brain is related to de-esterification to polar complex(es) for ECD (13) whereas it is linked to the reaction with glutathione for HMPAO (14). Several ECD imaging studies in normal subjects and patients showed that ECD clears slowly from the brain without any significant regional variations, i.e., equally from all regions of the brain including the white matter (11,15-18). The lack of differential elimination of ECD from the brain suggests that SPECT images obtained several hours postinjection can still reflect the initial activity pattern. However, there have also been a few studies suggesting that there may be some regional variation in ECD clearance (19-21).

The in vivo stability of tracer distribution may become a crucial issue in certain situations where SPECT imaging cannot be performed for several hours postinjection. For example, in epilepsy a significant delay in imaging may be necessary after ictal tracer injection because patients might be transferred from the EEG-monitoring unit to the imaging department or the camera might be busy with other patients (8). A similar situation may arise for patients with acute ischemic stroke where earliest rCBF measurements are desired but emergency treatment measures may preclude immediate scanning (22). Previously, we evaluated the feasibility of rCBF imaging of subjects in different stages of sleep by administering ECD at night during sleep and performing SPECT imaging conveniently in the morning when subjects awaken (23). To closely examine the issue of in vivo stability of ECD, we evaluated the

Received Aug. 28, 1996; revision accepted Jan. 7, 1997.

For correspondence or reprints contact: Masanori Ichise, MD, FRCP(C), Rm. 635, Nuclear Medicine, Department of Medical Imaging, Mount Sinai Hospital, 600 University Ave., Toronto, Ontario, Canada M5G 1X5.

regional ECD clearance and the temporal change in image contrast by performing serial ECD SPECT scans over 8 hr in 20 normal subjects.

MATERIALS AND METHODS

Subjects

Twenty age matched (10 men, mean age 35.5 ± 8.3 yr; 10 women, mean age 35.3 ± 10.2 yr) healthy volunteers participated in this study. They had no current or past history of neuropsychiatric disorders, major medical diseases or traumatic brain injury based on a screening interview and they were free of any drugs. They all gave written informed consent. The project was approved by the Human Subjects Review Committee of the University of Toronto.

SPECT Imaging

SPECT imaging was performed using a triple-head system equipped with ultra-high-resolution, fan-beam collimators and interfaced to a dedicated computer. ECD was prepared and quality control measures were performed according to the manufacturer's instructions. Each subject received an injection of 740 MBq (20 mCi) of ECD in a quiet room with the subject's eyes open and ears unplugged. Before imaging, four fiducial markers containing 55.5 kBq ($1.5 \mu\text{Ci}$) $^{99\text{m}}\text{Tc}$ were taped, two on each side of the subject's head at the level of the canthomeatal line (CML). A total of six serial scans were acquired for each subject starting at 30, 60, 120, 240, 360 and 480 min postinjection. For each scan, 120 36-sec projection images were obtained using a continuous scan mode at 3° angle intervals over 360° on a 128×128 matrix by rotating each head 120° (24 min per scan). The radius of rotation was fixed at 13.5 cm. Using a Jaszczak phantom (model 7000, Data Spectrum Corporation, Chapel Hill, NC) and capillary $^{99\text{m}}\text{Tc}$ line sources, FWHM was 9.0 mm in water at the center of the field of view.

One-pixel thick transaxial slices from the vertex of the brain to the level of the CML were reconstructed using a three-dimensional Butterworth postreconstruction filter (order = 6, cutoff frequency = 0.30) after applying a ramp back projection filter. Attenuation correction was performed by assuming uniform attenuation ($\mu = 0.09 \text{ cm}^{-1}$) (24) within an ellipse drawn around the skull as identified by the fiducial markers. Images were then reformatted to yield one-pixel thick (2.17 mm) transoblique slices parallel to the CML as identified by the fiducial markers.

To monitor system sensitivity, each of five plastic cylindrical phantoms [60 cm (2) \times 20 cm = 1200 ml] filled with a uniform solution of varying activities [7.4–185 MBq (0.2–5 mCi)] of $^{99\text{m}}\text{Tc}$ was scanned on selected days of experiment. The mean sensitivity of the system was $624 \pm 13 \text{ cpm}/\mu\text{Ci}$ and varied $<1\%$ ($n = 8$) and 4% ($n = 5$) within and between the experiments, respectively. Dead-time count losses over this activity range were negligible. In addition, the quantitative relationship between radioactivity and measured counts in the reconstructed image was evaluated by examining the phantom data processed with the same reconstruction parameters used in this study. This relationship was linear ($16.8 \pm 1.6 \text{ counts/pixel}/\mu\text{Ci}$) and varied less than 10% over the count range encountered in this study (70–1300 counts/pixel).

Quantitative SPECT Measurements

To obtain quantitative information on regional ECD activity, four sets of five consecutive transoblique slices (10.85 mm) were summed corresponding to the slice levels 3–4, 5–6, 7–8 and 11 in the Talairach's Co-planar Stereotaxic Atlas (25), respectively, using a modification of our previously reported method (26). Additionally, five consecutive slices corresponding to the highest signal in the basal ganglia and thalami were summed, respectively. Regions of interest (ROIs) were placed using elliptical or rectangular templates over the following regions: superior frontal (SF),

middle frontal (MF), inferior frontal (IF), cingulate gyrus (CG), anterior temporal (AT), posterior temporal (PT), parietal (PA), association cortex (AC), superior occipital (SO), inferior occipital (IO), cerebellum (CE), basal ganglia (BG), thalamus (TH) and white matter (WM) regions in each hemisphere (Fig. 1). These templates ranged in volume from 1.43 cm³ (TH) to 6.64 cm³ (BG) and were fixed in size across studies. ROI placement depended on visual identification of anatomical regions aided by the stereotaxic atlas. All ROIs were applied by the same investigator to eliminate the interoperator variation. The average coefficient of intraoperator variability in the quantitative measurements using this method was $2.0\% \pm 0.7\%$ ($n = 10$ trials, 28 regions). For the subsequent analysis, the following selected regions singly or in combination in each hemisphere were defined: frontal (IF + MF + IF), temporal (AT + PT), parietal (PA + AC), occipital (SO + IO), cerebellum (CE), basal ganglia (BG), thalamus (TH) and white matter (WM). Average counts per pixel from each region were decay-corrected to the time of the first scan at 30 min postinjection. No attempts were made to correct for partial volume or scatter effects.

To determine regional ECD clearance rates, regional time activity data were normalized to the corresponding counts in the first scan and were fitted to monoexponential and a sum of two exponentials using a nonlinear curve fitting technique (27). A comparison of goodness of fit between the two fits using the F-test (28) showed that the sum-of-two-exponential fit was superior to the monoexponential fit in only one region out of 48 regions in three subjects. Therefore, the monoexponential fit was selected for all subjects. Regional ECD clearance rates (%/hr) were then calculated in each patient from the time constants of the fitted monoexponentials.

To evaluate potential changes in the regional ECD distribution pattern with time, two sets of activity ratio measurements were made including gray-to-white matter (G/W) and gray-to-cerebellum (G/C) ratios. For these measurements, average counts per pixel from each region, averaged between the two hemispheres, were used.

Data Analysis

Because the parametric statistical tests used in this study require the assumption of normally distributed data, the regional ECD clearance rates and ratio measurements were tested for normality by calculating *w* statistics (Shapiro-Wilk's *W* test) (29). Analysis of variance (ANOVA) was used to compare ECD clearance rates and regional activity ratio measurements between groups. For the clearance analysis, the design included three between-groups factors: gender (male and female), region (frontal, temporal, parietal, occipital, cerebellum, basal ganglia, thalamus and white matter) and hemisphere (right and left). Hemisphere was treated as a repeated-measure factor and age was treated as a covariate. Multivariate analysis of covariance (MANCOVA) was also used to analyze associations between age and ECD clearance rates. For the ratio analysis, the design included two between-groups factors: region and scan time (30, 60, 120, 240, 360 and 480 min). Time was treated as a repeated-measure factor. Assuming no a priori hypothesis about the difference in ECD clearance rates or ratio measurements between groups, posthoc comparisons of group means were made using Scheffe tests (29) to correct for multiple comparisons. Statistical significance was defined as $p < 0.05$. Summaries of study variables were expressed as mean \pm s.d. All statistical analyses were implemented in STATISTICA (StatSoft, Inc., Tulsa, OK).

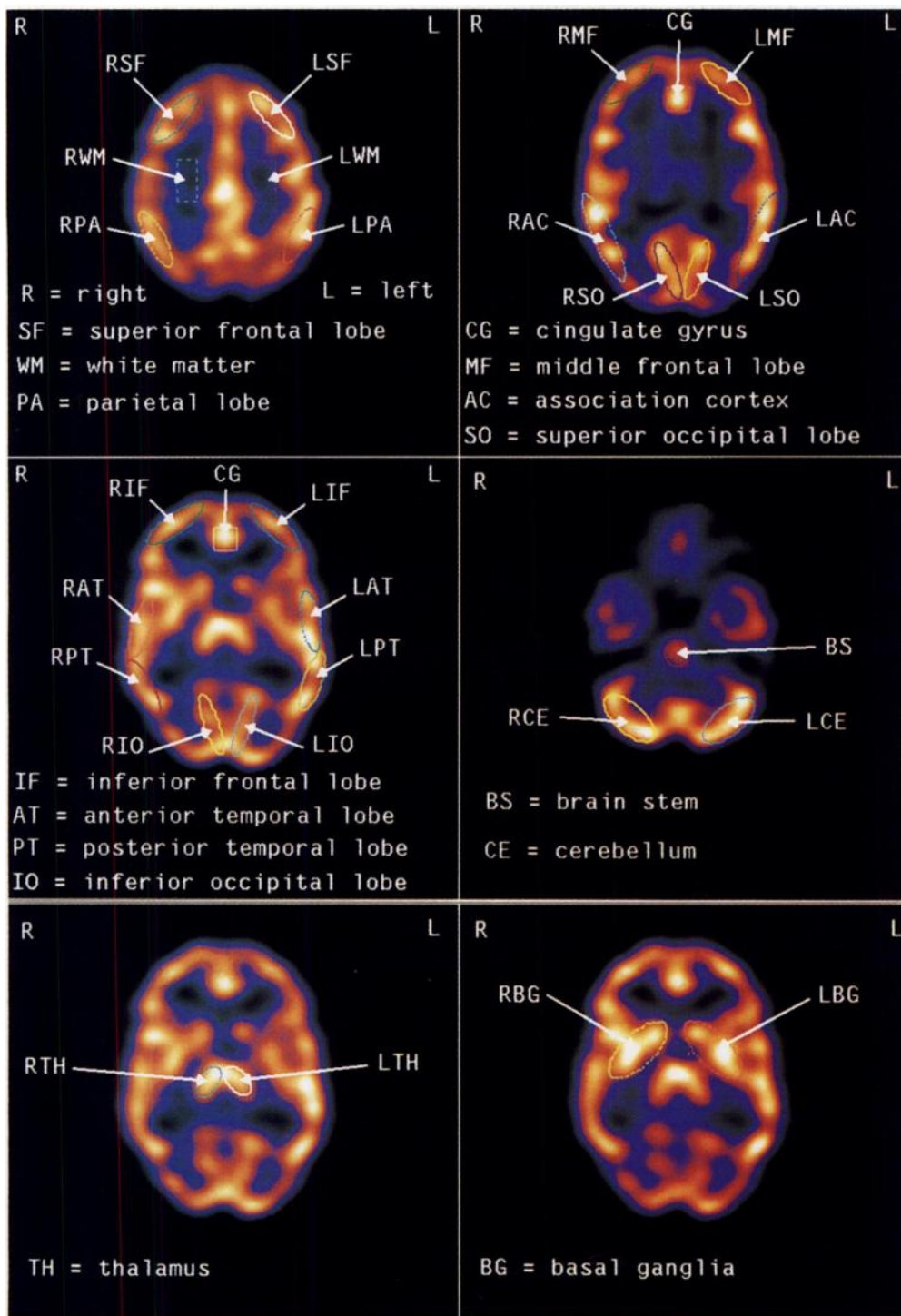


FIGURE 1. Region of interest templates based on a modification of the Talairach's Co-planar Stereotaxic Atlas (25).

RESULTS

The radiochemical purity of ECD was $98.3\% \pm 0.8\%$. Total counts per SPECT scan were 5.1 ± 2.9 million counts (range 1.2–13.8 million counts). All SPECT studies were technically adequate. The average ECD clearance from the overall brain was slow at $4.3\% \pm 1.7\%/hr$. Individual values of the ECD clearance rate averaged between the two hemispheric regions are summarized in Table 1 and the mean regional values are depicted in Figure 2. Serial ECD SPECT images of a 32-yr-old woman (Subject 14) are shown in Figure 3.

The regional ECD clearance rates and regional ratios were all normally distributed. There was a trend toward a higher overall ECD clearance for women ($4.50\% \pm 1.69\%/hr$) compared with men ($4.16\% \pm 1.70\%/hr$) but this difference did not reach

statistical significance ($F_{(1,143)} = 3.6, p = 0.06$). Region showed a highly significant main effect on ECD clearance ($F_{(7,143)} = 28.4, p < 10^{-5}$). None of the effects of hemisphere or the interactions between grouping factors was significant ($p = 0.1-0.6$). Age showed no significant association with regional ECD clearance rates (MANCOVA: $p = 0.14$). Regionally, the mean value of ECD clearance was higher for occipital ($6.34\% \pm 1.21\%/hr$) compared with the other regions ($p < 0.01$) except for frontal ($5.44\% \pm 1.11\%/hr$). The mean values of ECD clearance for both white matter ($2.39\% \pm 1.57\%/hr$) and thalamus ($2.45\% \pm 0.94\%/hr$) were lower ($p < 0.005$) compared with the other regions. Thus, ECD clearance showed a significant regional variation. The image effect of this regional variation in ECD clearance, particularly that of faster

TABLE 1
Regional ECD Clearance Rates (%/hr) in 20 Healthy Brains

Subjects no.	Age (yr)	Sex	Region							
			Frontal	Temporal	Parietal	Occipital	Cerebellum	Basal ganglia	Thalamus	White matter
1	25	M	5.16	4.53	4.04	6.35	4.13	4.41	1.76	1.46
2	40	M	5.18	4.51	4.04	6.27	4.13	4.41	1.76	1.95
3	32	M	4.51	4.36	3.44	6.17	4.98	4.19	1.19	2.88
4	40	M	4.16	4.51	3.96	4.60	3.02	4.13	1.81	1.99
5	45	M	6.39	5.08	5.41	7.44	6.09	4.69	2.41	2.09
6	29	M	4.08	3.78	3.39	5.75	2.71	4.33	1.25	1.42
7	26	M	5.19	4.43	4.86	6.34	3.79	5.22	2.49	1.54
8	28	M	5.87	5.93	5.61	7.58	6.02	5.34	3.38	1.39
9	44	M	6.40	5.68	6.56	7.61	5.93	4.92	3.04	1.44
10	46	M	4.98	4.11	3.28	5.41	3.09	3.07	1.28	0.56
11	47	F	5.86	5.59	4.71	6.62	4.86	4.61	3.52	3.94
12	41	F	7.22	3.78	5.94	8.69	5.40	5.41	3.63	0.63
13	32	F	4.40	3.37	3.19	5.01	2.74	2.68	1.97	4.39
14	32	F	7.87	7.07	6.36	7.98	4.97	6.61	1.64	1.37
15	26	F	5.24	5.14	3.98	6.14	4.10	5.62	3.75	5.44
16	19	F	6.05	5.64	4.82	7.25	4.07	6.22	4.26	5.72
17	41	F	6.63	5.86	5.36	7.08	4.51	5.84	3.18	3.88
18	42	F	5.62	4.40	3.94	4.67	4.34	4.42	2.74	3.15
19	24	F	3.92	3.14	2.61	4.30	2.42	3.49	2.39	2.39
20	49	F	4.01	3.12	3.34	5.47	3.34	3.37	1.57	0.24
Mean	35.4		5.44	4.70	4.44	6.34*	4.23	4.65	2.45 [†]	2.39 [‡]
s.d.	9.1		1.11	1.04	1.14	1.21	1.13	1.03	0.94	1.57

*Significantly higher ($p < 0.01$) compared with the other regions except for frontal.

[†]Significantly lower ($p < 0.005$) compared with the other regions except for white matter.

[‡]Significantly lower ($p < 0.005$) compared with the other regions except for thalamus.

and slower clearance from occipital region and thalamus or white matter, respectively, is illustrated in Figure 3.

For G/W ratios, the two between-groups factors (region and time) and the interaction between region and time were all highly significant ($p < 10^{-5}$). The mean values of regional G/W ratios are summarized in Table 2 and depicted in Figure 4. The overall mean G/W ratio at 30 min (2.13 ± 0.25) was not significantly different from that at 60 min (2.12 ± 0.23) but the ratio became progressively lower ($p < 10^{-6}$) thereafter, reaching 1.78 ± 0.23 at 480 min (Table 2 and Fig. 4). Except for

thalamus, none of the regional G/W ratios at 30 min were significantly different from the corresponding ratios at 60 min but they became progressively lower ($p < 0.05$) thereafter (Table 2, Fig. 4). The G/W ratio for occipital declined most with time (Fig. 4). On the other hand, the G/W ratio for thalamus was not significantly different between scans ($p = 0.06-0.90$) because the ECD clearance was equally slower for both white

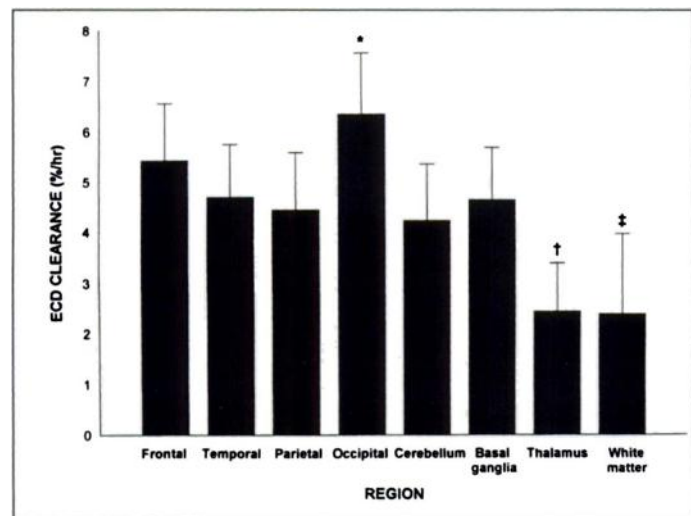


FIGURE 2. Mean regional ECD clearance rates in 20 healthy brains. *Significantly higher ($p < 0.01$) compared with the other regions except for frontal. [†]Significantly lower ($p < 0.005$) compared with the other regions except for white matter. [‡]Significantly lower ($p < 0.005$) compared with the other regions except for thalamus. Error bars are positive s.d.

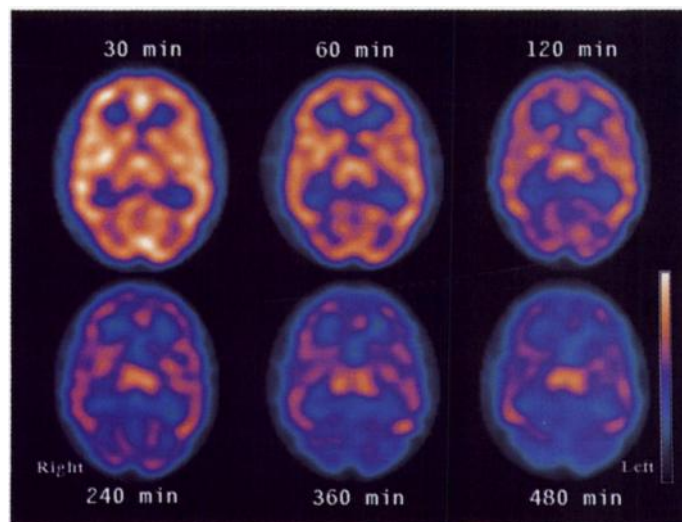


FIGURE 3. Serial ECD SPECT images (30–480 min postinjection) of a 32-yr-old woman (Subject 14) at the level of the thalamus. Images have been decay corrected to the time of the first scan. Small but significant overall ECD activity clearance is apparent. Significant reduction in the overall gray-to white matter contrast is apparent at 120 min and thereafter. Regionally, the activity in thalamus shows a relative increase with time but the activity in the frontal and occipital regions show a relative decrease with time. For identification of anatomical regions, refer to Figure 1.

TABLE 2
Gray-to-White Matter (G/W) Ratios

Time (min)	Region						
	Frontal	Temporal	Parietal	Occipital	Basal ganglia	Thalamus	Mean
30	2.02 ± 0.24	2.05 ± 0.20	2.05 ± 0.19	2.37 ± 0.26	2.14 ± 0.20	2.15 ± 0.24	2.13 ± 0.25
60	2.02 ± 0.22	2.05 ± 0.21	2.05 ± 0.20	2.33 ± 0.23	2.11 ± 0.20	2.17 ± 0.17	2.12 ± 0.23
120	1.92 ± 0.22*	1.97 ± 0.21*	1.97 ± 0.22*	2.19 ± 0.24*	2.03 ± 0.20*	2.13 ± 0.22	2.03 ± 0.24*
240	1.83 ± 0.22*	1.89 ± 0.17*	1.90 ± 0.19*	2.06 ± 0.15*	1.97 ± 0.18*	2.17 ± 0.21	1.97 ± 0.22*
360	1.73 ± 0.20*	1.79 ± 0.15*	1.85 ± 0.16*	1.91 ± 0.18*	1.91 ± 0.18*	2.16 ± 0.18	1.89 ± 0.22*
480	1.59 ± 0.17*	1.68 ± 0.13*	1.74 ± 0.17*	1.77 ± 0.17*	1.79 ± 0.17*	2.08 ± 0.21	1.78 ± 0.23*

*Significantly lower ($p < 0.05$) compared with the ratio at 30 min in the corresponding region.

matter and thalamus compared with the other regions (Table 2, Fig. 4).

For G/C ratios, the two between-groups factors (region and time) and the interaction between region and time were also all highly significant ($p < 10^{-5}$). The mean values of G/C ratios are summarized in Table 3 and depicted in Figure 5. The overall mean G/C ratios between 30 min (0.984 ± 0.095), 60 min (0.988 ± 0.097) and 120 min (0.973 ± 0.086) were not significantly different but the ratios at 240 min (0.955 ± 0.094), 360 min (0.965 ± 0.110) and 480 min (0.955 ± 0.115) were all lower ($p < 10^{-6}$) compared with the ratio at 30 min (Table 3, Fig. 5). Except for thalamus, none of the regional G/C ratios between 30 and 60 min for frontal and occipital and between 30, 60 and 120 min for temporal, parietal and basal ganglia were significantly different but they all became lower ($p < 0.05$) thereafter compared with the corresponding ratios at 30 min (Table 3, Fig. 5). The G/C for occipital declined most with time (Fig. 5). On the other hand, the G/C ratio for thalamus increased progressively from 0.995 ± 0.081 at 30 min to 1.120 ± 0.103 at 480 min ($p < 0.05$) because the clearance rate for cerebellum was significantly higher than for thalamus (Table 3, Fig. 5).

Thus, both G/W and G/C ratios showed a significant regional variation with time. The effect of relatively increasing activity in the thalamus and relatively decreasing activity in the occipital region with time on the image is illustrated in Figure 3.

DISCUSSION

Our finding of the overall ECD clearance of 4.3%/hr from healthy brains in this study is within the range of 0%–9%/hr for healthy brains or nonpathological brain regions reported by several

investigators (8,15,16,18,20,21,30,31) who used SPECT data. Planar imaging studies in the first hour, on the other hand, have found a significantly higher ECD clearance (16%–20%/hr) due to inclusion of rapidly clearing scalp activity (1,32). This soft tissue clearance of ECD was not assessed in this study because the first scan was obtained 30 min postinjection and no extracerebral ROI's were included in the study design.

Somewhat different clearance rates reported between studies may be related to differing methodological factors such as instrumentation (single versus multiheaded cameras), scan timing, image reconstruction parameters, filters, methods of quantitative measurement and data analysis, and/or biological factors such as age. The study by Pupi et al. (30) is one report in which no significant clearance of ECD from the brain was noted but the clearance was measured over only a 25-min interval in their study. In the majority of the studies in which clearance was measured using data obtained over several hours, the clearance was 5%–6%/hr (8,15,16,20,21). In this study, serial scans were obtained over 8 hr. In addition, we ensured that the count per pixel measurements made on reconstructed images were linear with radioactivity over the count range encountered. This is an important consideration for studies in which quantitative analysis of time activity data is performed.

In this study, there were no significant age- or gender-dependent changes in ECD clearance in our young normal controls. In the study reported by Ogawa et al. (20), the overall ECD clearance from the nonpathological brain regions of aged patients (66 ± 11 yr) with cerebrovascular diseases was 5.7%. Thus, ECD clearance appears independent of age even in advanced age. Pathological states of the brain, however, may have significant effects on the ECD clearance in the affected brain regions. Moretti et al. (31) noted differences between normal and ischemic regions where the ECD clearance was significantly greater in ischemic regions than in normal regions in early imaging periods (50–80 min). Grunwald et al. (8) also noted in their epilepsy studies that ECD clearance from hyperperfused seizure areas was significantly slower (1.3%/hr) compared to the overall brain (5.9%/hr). On the other hand, Ogawa et al. (20) noted that the defect-to-normal count ratio did not change over the 240-min period in patients with cerebrovascular diseases. Thus, further studies may be warranted to evaluate the in vivo stability of ECD in brain regions with various pathological conditions.

In contrast to other earlier studies (16–18), this study showed a small but significant regional difference in ECD clearance in normal brains, which is consistent with the findings reported recently (19–21). In particular, Yonekura et al. (19) noted relatively higher activity in the thalamus on delayed images at 4–5 hr in some patients. The discrepancy between the findings reported in the earlier studies and the latter including ours may be largely related to different instrumentation, i.e., lower spatial

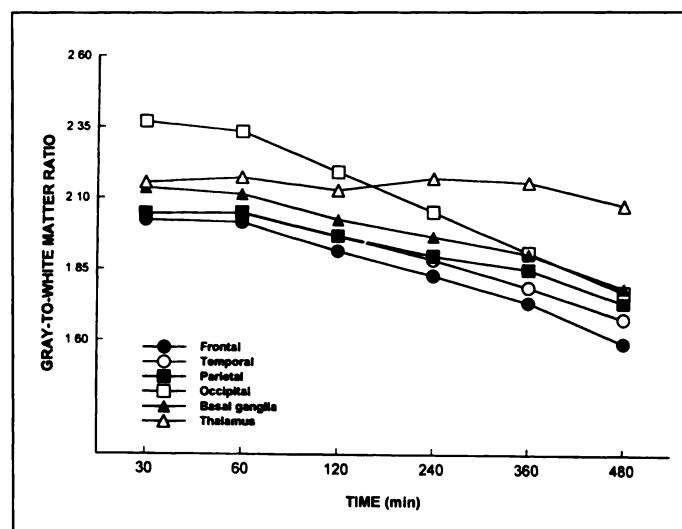


FIGURE 4. G/W ratios.

TABLE 3
Gray-to-Cerebellum (G/C) Ratios

Time (min)	Region						
	Frontal	Temporal	Parietal	Occipital	Basal ganglia	Thalamus	Mean
30	0.935 ± 0.092	0.945 ± 0.062	0.946 ± 0.069	1.093 ± 0.079	0.989 ± 0.089	0.995 ± 0.081	0.984 ± 0.095
60	0.939 ± 0.097	0.951 ± 0.065	0.953 ± 0.068	1.085 ± 0.079	0.985 ± 0.096	1.013 ± 0.095 [†]	0.988 ± 0.097
120	0.916 ± 0.085*	0.941 ± 0.064	0.941 ± 0.056	1.049 ± 0.067*	0.971 ± 0.078	1.020 ± 0.087 [†]	0.973 ± 0.086
240	0.886 ± 0.079*	0.915 ± 0.060*	0.920 ± 0.068*	1.000 ± 0.84*	0.956 ± 0.073*	1.056 ± 0.089 [†]	0.955 ± 0.094*
360	0.883 ± 0.091*	0.912 ± 0.065*	0.943 ± 0.073*	0.975 ± 0.088*	0.972 ± 0.088*	1.103 ± 0.107 [†]	0.965 ± 0.110*
480	0.858 ± 0.88*	0.904 ± 0.73*	0.932 ± 0.067*	0.955 ± 0.084*	0.962 ± 0.071*	1.120 ± 0.103 [†]	0.955 ± 0.115*

*Significantly lower ($p < 0.05$) compared with the ratio at 30 min in the corresponding region.

[†]Significantly higher ($p < 0.05$) compared with the ratio at 30 min in the corresponding region.

resolution systems for the former versus high resolution multi-headed systems for the latter. In this study, we found a significantly lower ECD clearance for both white matter and thalamus but a higher clearance for occipital. This differential ECD clearance may be related to rCBF differences, being higher for occipital but lower for white matter. However, it may be difficult to explain the slower clearance for thalamus based on the rCBF difference because rCBF is relatively high for thalamus. The thalamic ROI was smallest in volume (1.43 cm³)

compared with the other ROIs in this study. Thus, the clearance measurement might be affected by the partial volume effects from the adjacent white matter. This possibility, however, appears unlikely in this study because the effect of the slower ECD clearance in the thalamus was visually apparent as relatively increasing activity on tomographic images. Also, ECD clearance was slower in hyperperfused seizure areas in the ictal studies discussed elsewhere (8). ECD clearance therefore may be totally independent of rCBF. The reason for the

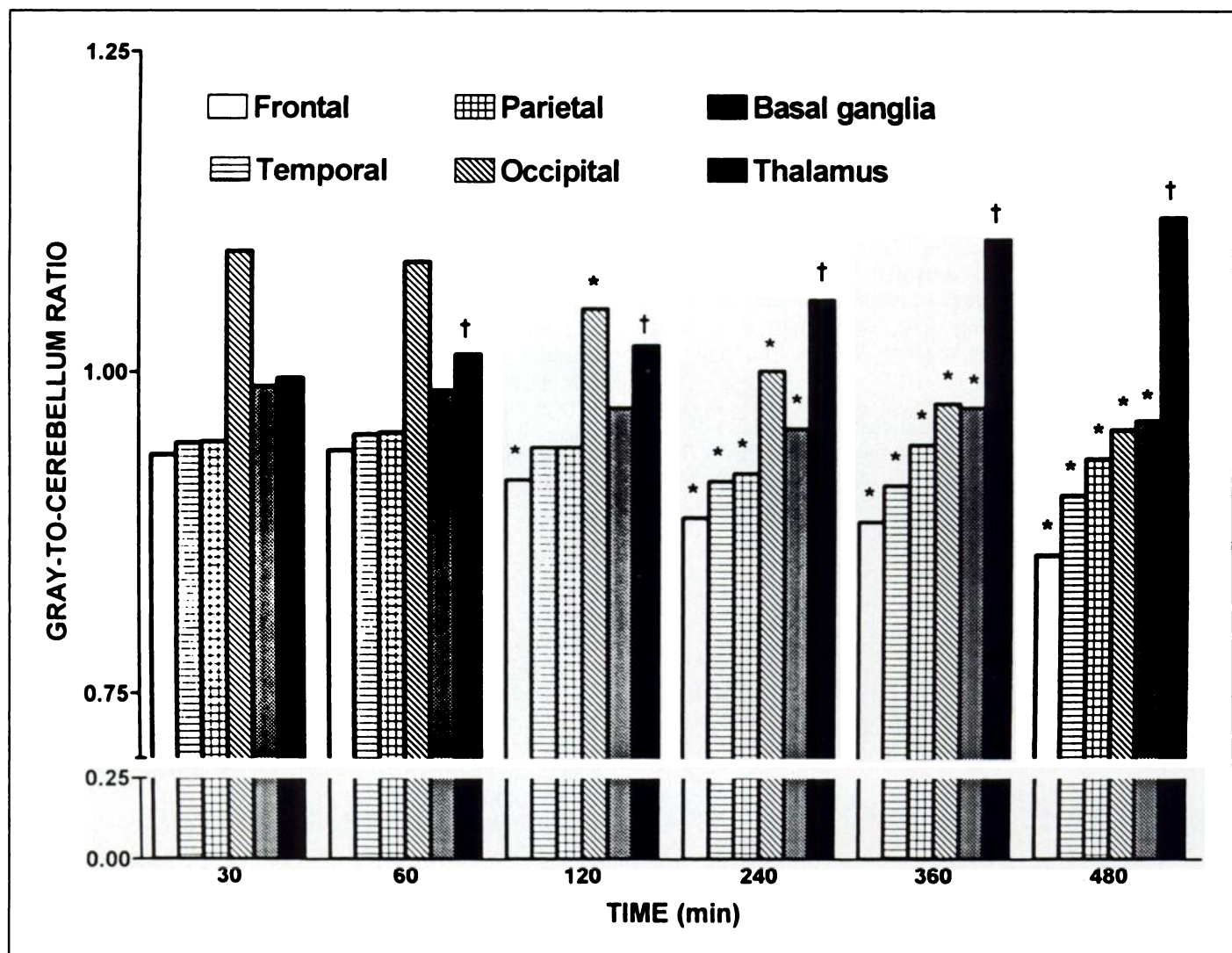


FIGURE 5. G/C ratios. * Significantly lower ($p < 0.05$) compared with the ratio at 30 min in the corresponding region. [†]Significantly higher ($p < 0.05$) compared with the ratio at 30 min in the corresponding region.

differential ECD clearance therefore is unclear. One may speculate that the underlying mechanism may be related to regional differences in esterase activity and/or blood-brain-barrier permeability, making egress of polar metabolites of ECD from certain regions such as thalamus somehow more difficult compared with other regions.

The regional changes with time in both the G/W and G/C ratios found in this study are a result of the regional variation of ECD clearance. Because the ECD clearance was equally slower for both white matter and thalamus compared with the other regions, the G/W ratio decreased with time for all other regions but the ratio for thalamus was unchanged. The G/C ratio for thalamus on the other hand increased with time because the clearance rate for cerebellum was significantly higher than for thalamus. Based on our findings, the optimal time to start ECD scanning may be between 30 and 120 min postinjection, consistent with the recommendation made in the NeuroLite® package insert (30–60 min postinjection), because the overall G/W ratio or the gray-to-white matter image contrast was reduced significantly from 120 min onward below 95% of the initial value. However, the overall gray matter distribution pattern as measured by the mean G/C ratio was stable up to 4 hr postinjection. Although neither the G/W nor G/C ratios significantly differed between 30 and 60 min, scanning before 30 min would not be recommended because of the presence of high blood pool activity (18).

HMPAO has been generally thought to be very stable in vivo with a clearance as low as 0.4%/hr (33). However, Suess et al. (34) evaluated the time-dependent release of HMPAO activity in vitro using cell culture of dissociated rat cerebellum, which was 16% after 2 hr. Recent work in our laboratory has shown that ECD clearance from cells in vitro is greater than that of HMPAO (unpublished data, 1997). Thus, future in vivo HMPAO studies as well as ECD/HMPAO comparison studies including both healthy and pathological brains may be warranted to address further the issue of the in vivo stability of these commonly used rCBF tracers. In contrast to ECD or HMPAO, [¹²³I]IMP, which is the first “retained-type” tracer introduced for SPECT rCBF imaging and is available in some countries, is known to show a more complex dynamic change in the regional distribution due to “redistribution” in addition to “washout” (35). It is, therefore, critical to perform IMP imaging early at 20 min postinjection (35).

CONCLUSION

ECD clears from normal brain slowly and shows a significant regional variation. As a result, G/W contrast begins to decrease after 2 hr and the gray-matter activity pattern becomes significantly different after 4 hr. Therefore, the optimal imaging time may be between 30–120 min postinjection. However, images obtained up to 4 hr still maintain the initial gray-matter activity pattern. Further studies may be warranted to evaluate the in vivo stability of ECD in different pathological brains.

ACKNOWLEDGMENTS

This work was supported by the SPECT Research Fund from the Department of Medical Imaging, Mount Sinai Hospital, partly contributed by DuPont Pharmaceutical, North Billerica, MA and Toronto Psychiatric Research Foundation, Toronto, Canada. H. Golan was partly supported by the Shiff Family Fund and the Doctor Abraham Shore Memorial Fund. We thank Kevin Hall at DuPont Pharmaceutical for his helpful suggestions. This work was presented in part at the 42nd Annual Meeting of the Society of Nuclear Medicine, Minneapolis, MN, June 12–15, 1995.

REFERENCES

- Vallabhajosula S, Zimmerman RE, Picard M, et al. Technetium-99m-ECD: a new brain imaging agent: in vivo kinetics and biodistribution studies in normal human subjects. *J Nucl Med* 1989;30:599–604.
- Brass LM, Walovitch RC, Joseph JL, et al. The role of single photon emission computed tomography brain imaging with ^{99m}Tc-bicisate in the localization and definition of mechanism of ischemic stroke. *J Cereb Blood Flow Metab* 1994;14(suppl 1):S91–S98.
- Moretti JL, Defer G, Tamgac F, Weinmann P, Belin C, Cesaro P. Comparison of brain SPECT using ^{99m}Tc-bicisate (_{L,L}-ECD) and [¹²³I]IMP in cortical and subcortical strokes. *J Cereb Blood Flow Metab* 1994;14(suppl 1):S84–S90.
- Nakagawara J, Nakamura J, Takeda R, et al. Assessment of postischemic reperfusion and diamox activation test in stroke using ^{99m}Tc-ECD SPECT. *J Cereb Blood Flow Metab* 1994;14(suppl 1):S49–S57.
- Lassen NA, Sperling B. Technetium-99m-bicisate reliably images CBF in chronic brain diseases but fails to show reflow hyperemia in subacute stroke: report of a multicenter trial of 105 cases comparing ¹³³Xe and ^{99m}Tc-bicisate (ECD, NeuroLite) measured by SPECT on same day. *J Cereb Blood Flow Metab* 1994;14(suppl 1):S44–S48.
- Tsuchida T, Nishizawa S, Yonekura Y, et al. SPECT images of technetium-99m-ethyl cysteinate dimer in cerebrovascular diseases: comparison with other cerebral perfusion tracers and PET. *J Nucl Med* 1994;35:27–31.
- Waldemar G, Walovitch RC, Andersen AR, et al. Technetium-99m-bicisate (NeuroLite) SPECT brain imaging and cognitive impairment in dementia of the Alzheimer type: a blinded read of image sets from a multicenter SPECT trial. *J Cereb Blood Flow Metab* 1994;14(suppl 1):S99–S105.
- Grunwald F, Menzel C, Pavics L, et al. Ictal and interictal brain SPECT imaging in epilepsy using technetium-99m-ECD. *J Nucl Med* 1994;35:1896–1901.
- Menzel C, Grunwald F, Pavics L, et al. Brain single-photon emission tomography using technetium-99m-bicisate (ECD) in a case of complex partial seizure. *Eur J Nucl Med* 1994;21:1243–1246.
- Packard AB, Roach PJ, Davis RT, et al. Ictal and interictal technetium-99m-bicisate brain SPECT in children with refractory epilepsy. *J Nucl Med* 1996;37:1101–1106.
- Walovitch RC, Franceschi M, Picard M, et al. Metabolism of ^{99m}Tc-_{L,L}-ethyl cysteinate dimer in healthy volunteers. *Neuropharmacology* 1991;30:283–292.
- Neirinckx RD, Canning LR, Piper IM, et al. Technetium-99m d,l-HM-PAO: a new radiopharmaceutical for SPECT imaging of regional cerebral blood perfusion. *J Nucl Med* 1987;28:191–202.
- Walovitch RC, Cheesman EH, Maheu LJ, Hall KM. Studies of the retention mechanism of the brain perfusion imaging agent ^{99m}Tc-bicisate (^{99m}Tc-ECD). *J Cereb Blood Flow Metab* 1994;14(suppl 1):S4–11.
- Neirinckx RD, Burke JF, Harrison RC, Forster AM, Andersen AR, Lassen NA. The retention mechanism of technetium-99m-HMPAO: intracellular reaction with glutathione. *J Cereb Blood Flow Metab* 1988;8:S4–S12.
- Franceschi M, Picard M, Zimmerman RE, Kronauge JF, Jones AG, Holman BL. Brain washout of ^{99m}Tc-_{L,L}-ethyl cysteinate dimer (ECD) in normal volunteers [Abstract]. *Eur J Nucl Med* 1988;14:227.
- Leveille J, Demonceau G, De Roo M, et al. Characterization of technetium-99m-_{L,L}-ECD for brain perfusion imaging, part 2. Biodistribution and brain imaging in humans [Abstract]. *J Nucl Med* 1989;30:1902–1910.
- Leveille J, Demonceau G, Walovitch RC. Intrastudy comparison between technetium-99m-ECD and technetium-99m-HMPAO in healthy human subjects. *J Nucl Med* 1992;33:480–484.
- Devous MD Sr, Payne JK, Lowe JL, Leroy RF. Comparison of technetium-99m-ECD to xenon-133 SPECT in normal controls and in patients with mild to moderate regional cerebral blood flow abnormalities. *J Nucl Med* 1993;34:754–761.
- Yonekura Y, Sasaki Y, Kubo A, Tanada S, Momose T, Torizuka K. Phase 2 clinical study of ^{99m}Tc-ECD: a multicenter study. *Kaku Igaku* 1992;29:1113–1125.
- Ogawa Y, Nishimura T, Hayashida K, et al. Cerebral perfusion scintigraphy in patients with cerebrovascular disease by using ^{99m}Tc-ECD: comparative study with ¹²³I-IMP SPECT. *Kaku Igaku* 1991;28:599–607.
- Matsuda H, Kinuya K, Higashi S, et al. Evaluation of brain perfusion SPECT imaging using ^{99m}Tc-ECD. *Kaku Igaku* 1991;28:701–709.
- Alexandrov AV, Grotta JC, Davis SM, Lassen NA. Brain SPECT and thrombolysis in acute ischemic stroke: time for a clinical trial. *J Nucl Med* 1996;37:1259–1262.
- Ichise M, Blackman A, Golan H, et al. SPECT imaging of regional cerebral blood flow during sleep in human using ^{99m}Tc-ECD [Abstract]. *J Nucl Med* 1995;36:245P.
- Chang L. A method for attenuation correction in radionuclide computed tomography. *IEEE Trans Nucl Sci* 1978;NS-25:638–643.
- Talairach J, Tournoux P, Rayport M. Co-planar stereotaxic atlas of the human brain. Three-dimensional proportional system: an approach to cerebral imaging. New York, NY: Thieme Inc.; 1988:1–122.
- Ichise M, Toyama H, Vines DC, Chung DG, Kirsh JC. Neuroanatomical localization for clinical SPECT perfusion brain imaging: a practical proportional grid method. *Nucl Med Commun* 1992;13:861–866.
- Levenberg K. A method for the solution of certain problems in least squares. *Q Appl Math* 1944;2:164–168.
- Landaw EM, DiStefano JJ. Multiexponential, multicompartmental and noncompartmental modeling. II. Data analysis and statistical considerations. *Am J Physiol* 1984;246:R665–R677.
- Basic statistics and tables. In: STATISTICA for Windows. Tulsa, OK: StatSoft Inc.; 1996:1301–1428.
- Pupi A, Castagnoli A, De Cristofaro MT, Bacciottini L, Petti AR. Quantitative comparison between ^{99m}Tc-HMPAO and ^{99m}Tc-ECD: measurement of arterial input and brain retention. *Eur J Nucl Med* 1994;21:124–130.
- Moretti JL, Tamgac F, Weinmann P, et al. Early and delayed brain SPECT with technetium-99m-ECD and iodine-123-IMP in subacute strokes. *J Nucl Med* 1994;35:1444–1449.

32. Holman BL, Hellman RS, Goldsmith SJ, et al. Biodistribution, dosimetry, and clinical evaluation of technetium-99m-ethyl cysteinyl dimer in normal subjects and in patients with chronic cerebral infarction. *J Nucl Med* 1989;30:1018-1024.
33. Andersen AR. Technetium-99m-HMPAO: basic kinetic studies of a tracer of cerebral blood flow. *Cerebrovasc Brain Metab Rev* 1989;1:288-318.

34. Suess E, Huck S, Reither H, Hortnagl H, Angelberger P. Uptake mechanism of technetium-99m-d,l-HMPAO in cell cultures of the dissociated postnatal rat cerebellum. *J Nucl Med* 1992;33:108-114.
35. Moretti JL, Caglar M, Weinmann P. Cerebral perfusion imaging tracers for SPECT: which one to choose? *J Nucl Med* 1995;36:359-363.

Fluorine-18-FPH for PET Imaging of Nicotinic Acetylcholine Receptors

Andrew Horti, Ursula Scheffel, Marigo Stathis, Paige Finley, Hayden T. Ravert, Edythe D. London and Robert F. Dannals
Intramural Research Program, National Institute on Drug Abuse, Baltimore, Maryland; and Division of Nuclear Medicine, Department of Radiology, The Johns Hopkins Medical School, Baltimore, Maryland

Visualization of central nicotinic acetylcholine receptors (nAChRs) with modern PET or SPECT imaging techniques has been hampered by the lack of a radioligand with suitable in vivo binding characteristics (i.e., high target-to-nontarget ratios and kinetics appropriate for the half-life of the tracer and imaging modality used). This paper describes in vivo binding, kinetics and pharmacology of a highly potent ^{18}F -labeled analog of epibatidine, (\pm)-exo-2-(2-[^{18}F]fluoro-5-pyridyl)-7-azabicyclo[2.2.1]heptane (^{18}F FPH), in the mouse brain with the view towards application of this tracer for PET imaging of nAChR in human brain. **Methods:** Fluorine-18-FPH was administered intravenously to mice, and time-activity curves were determined for several regions in the brain and other organs. Saturation and pharmacology of ^{18}F FPH binding was demonstrated in vivo by preinjecting unlabeled FPH or other drugs with known pharmacological action before ^{18}F FPH was injected. The effect of the drugs on ^{18}F FPH accumulation was evaluated. **Results:** ^{18}F FPH was rapidly incorporated into the mouse brain; peak activity (2.4% of the injected dose) was measured at 5 min after intravenous administration, followed by washout to 1.1% injected dose (ID) at 60 min. Highest concentrations of ^{18}F occurred at 15 min in areas known to contain high densities of nAChR (e.g., thalamus [9.7% of injected dose per gram tissue (ID/g)] and superior colliculus (8.3% ID/g)). Accumulation of the ^{18}F tracer in hippocampus, striatum, hypothalamus and cortical areas was intermediate (5.0, 5.6, 4.2 and 5.6% ID/g, respectively) and low in the cerebellum (2.8% ID/g). The distribution of ^{18}F FPH in the mouse brain matched that of other in vivo nAChR probes such as ^3H -labeled epibatidine or norchloroepibatidine, [^3H]-(-)-nicotine and [^3H]cytisine and that of nAChR densities determined in postmortem autoradiographic studies in rodents. Preinjection of blocking doses of unlabeled epibatidine, (-)-nicotine, lobeline and cytisine significantly inhibited ^{18}F FPH binding in thalamus and superior colliculus, but not in cerebellum, whereas drugs that interact with binding sites other than acetylcholine recognition sites of nAChR (e.g., mecamylamine, scopolamine, N-methylspiperone and ketanserin) had no effect on ^{18}F FPH accumulation in any of the brain regions examined. **Conclusion:** Fluorine-18-FPH labels nAChR in vivo in the mouse brain. Because of its high uptake into the brain and high ratios of specific-to-nonspecific binding, this radioligand appears to be ideally suited for PET imaging of nAChR in the mammalian brain.

Key Words: nicotinic acetylcholine receptor; brain imaging; PET

J Nucl Med 1997; 38:1260-1265

Cerebral nicotinic acetylcholine receptors (nAChRs), important sites of excitatory neurotransmission in brain, have been

studied extensively. Molecular biological techniques have been applied in determining the amino acid sequences of the subunits that compose the receptor (1-3), autoradiographic techniques have been used to delineate the anatomical distribution of nAChRs in brain (4-7) and metabolic mapping studies have demonstrated that the specific binding sites labeled in brain with specific radioligands are coupled to functional activity (8). Human investigations have provided evidence for a critical role of nAChRs in cognition and in the pathogenesis of Alzheimer's (9) and Parkinson's diseases (10). Furthermore, nAChRs are the sites of action of nicotine, the ingredient that promotes tobacco addiction, a disorder to which over 400,000 deaths a year are attributed in the U.S. (11).

Despite the critical function of nAChRs in normal physiology and in disorders of brain function, a suitable probe for assaying this receptor noninvasively in the human brain is not available. (-)-S-[$^{11}\text{CH}_3$]Nicotine has been used to image nAChRs in monkey (12,13) and human (14) brain using PET. Studies of patients with Alzheimer's disease showed less uptake of both (+)-(R)- and (-)-S-[$^{11}\text{CH}_3$]nicotine in the brain as compared with uptake in age-matched controls, consistent with the profound loss of nAChRs in postmortem material from patients who died with the disease (15,16). Nonetheless, rapid egress of radiolabeled nicotine from the brain and high levels of nonspecific binding (7,14) limit the utility of isotopically labeled nicotine as a tracer for PET. Another nicotinic agonist, [^3H]cytisine, has been evaluated for the purpose of in vivo labeling of nAChRs in mouse brain (17). Although this ligand has a slower clearance from brain than does [^3H]nicotine, and considerably less nonspecific binding, relatively poor penetration of the blood-brain barrier suggested that labeling cytisine for PET studies would not be worthwhile.

Impetus for further work on development of radioligand probes for in vivo labeling of nAChRs has been provided by the discovery of epibatidine, an alkaloid extracted from the skin of the Ecuadorian poisonous frog *Epipedobatus tricolor* (18) and its characterization as (+)-exo-2-(2-chloro-5-pyridyl)-7-azabicyclo[2.2.1]heptane (19,20). Studies in mice demonstrated that peripherally administered epibatidine was an extremely potent antinociceptive agent, suggesting a central action (21), and its structural similarity to nicotine suggested that the alkaloid might have activity at nAChRs (22). Indeed, the latter hypothesis was confirmed in receptor binding assays indicating that epibatidine inhibited the binding of [^3H]nicotine and [^3H]cytisine but not that of radioligands selective for a variety of other neurotransmitter receptors (21,23-25). Both enantiomeric forms of epibatidine, the natural (+)- and the

Received July 11, 1996; revision accepted Nov. 14, 1996.
For correspondence or reprints contact: Ursula Scheffel, Sc D, Nuclear Medicine Research, 220 Ross Research, The Johns Hopkins Medical School, 720 Rutland Avenue, Baltimore, MD 21205-2196.